Journal of Catalysis 276 (2010) 215–228

Contents lists available at ScienceDirect

Journal of Catalysis

journal homepage: www.elsevier.com/locate/jcat

Effects of support composition and pretreatment on the activity and selectivity of carbon-supported $PdCu_nCl_x$ catalysts for the synthesis of diethyl carbonate

Daniel N. Briggs, Gerry Bong, Eric Leong, Kevin Oei, Gabriella Lestari, Alexis T. Bell *

Department of Chemical Engineering, University of California, Berkeley, CA 94720, USA

ARTICLE INFO

Article history:
Received 30 April 2010
Revised 2 August 2010
Accepted 3 August 2010
Available online 10 November 2010

Keywords:
Diethyl carbonate
Carbon nanofibers
Activated carbon
Copper chloride
Palladium chloride

ABSTRACT

The oxidative carbonylation of ethanol to diethyl carbonate (DEC) has been investigated on catalysts prepared by dispersing $CuCl_2$ and $PdCl_2$ on activated carbon and carbon nanofibers. The objectives of this work were to establish the effects of support structure and pretreatment on the dispersion of the catalytically active components and, in turn, on the activity and selectivity of the catalyst for DEC synthesis. At the same surface loading of $CuCl_2$ and $PdCl_2$, partially oxidized carbon nanofibers resulted in a higher dispersion of the active components and a higher DEC activity than could be achieved on activated carbon. Catalyst characterization revealed that nearly atomic dispersion of $CuCl_2$ and $PdCl_2$ could be achieved on the edges of the graphene sheets comprising the carbon nanofibers. Over oxidation of the edges or their removal by heat treatment of the nanofibers resulted in a loss of catalyst activity. The loss of catalyst activity with time on stream could be overcome by the addition of ppm levels of CCl_4 to the feed. While catalysts prepared with $CuCl_2$ alone were active, a fivefold increase in activity was realized by using a $PdCl_2/CuCl_2$ ratio of 1/20. It is proposed that the Pd^{2+} cations interact with $[CuCl_2]^-$ anions to form $Pd[CuCl_2]_2$ complexes that are stabilized through dative bonds formed with oxygen groups present at the edges of the graphene sheets of the support. A mechanism for DEC synthesis is discussed, and a role for the Pd^{2+} cations as part of this mechanism is proposed.

1. Introduction

Diethyl carbonate (DEC) is a potential fuel oxygenate, which possesses lower volatility, better fuel/water partitioning coefficient, and more benign hydrolysis products than dimethyl carbonate (DMC), while retaining similar blending octane properties [1,2]. Commercial production of DEC and other alkyl carbonates can be carried out by oxidative carbonylation of the appropriate alcohol Eq. (2) in a slurry containing cuprous chloride to catalyze the reaction [3].

$$2ROH + CO + \frac{1}{2}O_2 \xrightarrow{CuCl} (RO)_2CO + H_2O \quad (1)$$

Inherent difficulties with the slurry process (e.g. corrosion and product separation) have motivated efforts to develop a heterogeneous catalyst for gas-phase synthesis of alkyl carbonates. To this end, investigations have been carried out using $CuCl_2$ and CuCl in combination with $PdCl_2$ and other additives such as KCl and NaOH supported on activated carbon (AC) [4–13], silica [7,14,15], alumina [7,16], and zeolites [17–20]. Of the systems studied, AC-supported catalysts have been found to be the most active and selective to alkyl carbonates. However, the stability of such catalysts is an issue, and the observed loss of activity with time on stream has been attributed to the loss of Cl [4,5,10,13]. Several studies have shown that catalyst activity can be restored by ex situ regeneration using HCl [4,5], but continuous regeneration of catalyst activity by the addition of HCl or other Cl-containing compounds to the feed has only been successful for an alumina-supported catalyst [16].

AC-supported catalysts have usually been made by impregnating the support with an aqueous solution of $CuCl_2$ and promoters (including $PdCl_2$, alkali chlorides, and alkali hydroxides) [7,13]. While it has been established that the promoters enhance catalyst activity and alkyl carbonate selectivity, relatively little is known about structure of the active species. In a recent report, we have presented details about the structure of the active species in a $KCl–NaOH–PdCl_2–CuCl_2$/AC catalyst, obtained using X-ray absorption spectroscopy and electron microscopy [13]. While $CuCl_2$ was used as a precursor, virtually all of the Cu was present as very highly dispersed Cu(I) species after catalyst use. Information obtained from Cu K-edge XANES and EXAFS, and from Cl K-edge XANES suggest that the Cu^+ cations exist as linear $[CuCl_2]^-$ anions. Pd was present exclusively as $PdCl_2$, mostly in the form of 30 nm crystallites. The interaction between cuprous chloride and KCl was thought to lead to the formation of potassium chlorocuprate compounds, which melt at the reaction temperature (423 K) and could increase the mobility and Cl coordination of Cu. DEC activity

* Corresponding author. Address: 107 Gilman Hall, Department of Chemical Engineering, UC Berkeley, Berkeley, CA 94720, USA. Fax: +1 510 642 4778.
E-mail address: bell@cchem.berkeley.edu (A.T. Bell).

0021-9517/$ - see front matter © 2010 Elsevier Inc. All rights reserved.
doi:10.1016/j.jcat.2010.08.004

was attributed primarily to interactions between $[CuCl_2]^-$ and $PdCl_2$, since both are required for high activity. An important conclusion of this study was the recognition that the low dispersion of $PdCl_2$ limited the interactions of $[CuCl_2]^-$ anions with $PdCl_2$ and, hence, the activity and selectivity of the catalyst for DEC formation.

Previous investigations have shown that dispersion of $PdCl_2$ on carbon supports is highly dependent on structure and pretreatment of the support [21,22]. AC has a highly irregular structure and morphology, making it difficult to relate activity to specific types of precursor–support interactions. By contrast, carbon nanofibers (CNF) have a significantly more regular structure and can be prepared with moderately high surface areas (up to 250 m^2/g). Moreover, CNF can be grown to preferentially expose either the edge planes (platelet or fish-bone carbon nanofibers) or basal planes (parallel carbon nanofibers) of graphene [23,24]. Prior work has also shown that the dispersion of $PdCl_2$ on both AC- and CNF-type supports can be controlled by partial oxidation of the edges of the graphene sheets [25,26].

The present study was undertaken: (1) to determine the influence of carbon support properties on the activity of carbon-supported $PdCu_nCl_x$ catalysts for DEC synthesis; (2) to describe more precisely the nature of the active species and its interaction with the carbon support; and (3) to identify means for stabilizing catalyst activity. The catalytic activities of several carbon-supported catalysts were compared, and accompanying structural characterization was used to rationalize differences in activity. The extent of oxidation of the carbon support was established as an important parameter in determining catalyst activity and stability. Scanning electron microscopy and high resolution transmission electron microscopy were used to assess the uniformity of catalyst dispersion over the carbon surfaces. Increased $PdCl_2$ dispersion resulted in higher DEC activity, as suggested by our prior work. Insights from catalysis, catalyst characterization, and the literature led to the development of a new model for the active species, along with a mechanism for cooperation between CuCl and $PdCl_2$.

2. Experimental

2.1. Catalyst preparation

Darco activated carbon (Aldrich, 12–20 mesh) and heat-treated carbon nanofibers (CNF-HT, Strem) were hand ground to ~100 mesh before further use; acid-washed carbon nanofibers (CNF, Strem) were received as a ~120 mesh powder and were used as received. Both types of fibers were grown by the same process, but then subjected to two different treatments [27,28]. Acid washing removed the Ni/MgO catalyst used to grow the fibers, whereas heat treatment induced partial graphitization, increasing the ratio of basal to edge surface area of the nanofibers. Table 1 lists the BET surface areas of the supports used in this study.

The effect of mild or strong surface oxidation was investigated by pretreating the acid-washed carbon nanofiber (CNF) in 0.5 M HNO_3 (mild oxidation) or a 1:1 mixture of concentrated HNO_3 and H_2SO_4 (strong oxidation). The conditions chosen for oxidation of the support were based on previously reported studies [22,25]. Oxidation was carried out by contacting acid-washed nanofibers in a round-bottomed flask with a solution of the desired acid (25 mL solution/g carbon). This mixture was stirred and heated at reflux (368–373 K) for 1 h, then filtered and washed until the filtrate was neutral. Supports thus oxidized were then dried overnight at 383 K.

$CuCl_2$ (anhydrous, Acros), $PdCl_2$ (Aldrich), and KCl (Fisher) were introduced onto the carbon supports by incipient wetness impregnation (IWI), using an aqueous solution of each salt or mixture of salts. While cuprous species are known to catalyze the oxidative carbonylation of alcohols (see Section 1), the solubility of CuCl in aqueous solution is poor, while $CuCl_2$ dissolves readily. As we have reported previously, the interactions of the $CuCl_2$ precursor with the support results in the reduction of $CuCl_2$ to cuprous chloride species [13]. Details of the reduction process are presented in Section 4.

The amount of solution needed to wet each support (1.7 mL H_2O/g AC; 1.5 mL H_2O/g carbon nanofibers) was determined by dropwise addition of water to the support until the onset of visible wetness. Catalyst loadings were adjusted according to the surface area of the support (Tables 1 and 2). Complete dissolution of the precursors (especially $PdCl_2$) took several hours and was sometimes assisted by sonication. The resulting homogeneous green–brown solution of $CuCl_2$, $PdCl_2$, and KCl was added dropwise under ambient conditions to the support, which was pre-dried at 383 K. To ensure uniform distribution of the precursors over the support surface, the powder was mixed thoroughly after every 3–5 drops of solution. Any excess liquid was removed under gentle nitrogen flow while stirring. The catalyst was dried for 5 h at 383 K in air and then stored at room temperature until use. The preparation conditions for catalysts in this study are summarized in Table 2.

2.2. Catalytic activity and selectivity

The apparatus used to investigate catalyst activity and selectivity was identical to that described previously [13]. Because the catalyst activity and selectivity changed during the course of the reaction, a new sample of catalyst was used for each experiment.

Table 1
Summary of carbon supports used in this study.

Carbon type	Abbreviation	Surface area (m^2/g)
Carbon nanofibers (acid washed)	CNF	120
Carbon nanofibers (heat treated)	CNF-HT	120
Activated carbon	AC	545

Table 2
Summary of catalysts prepared in this study. The metal loadings (in wt.%) are those used during impregnation.

Catalyst designation	$CuCl_2$[a]	$PdCl_2$[a]	Cu/Pd[b]	KCl[c]	Notes
KCP/AC	3.0	0.25	20	1.0	
KCP/CNF	0.66	0.06	19	1.0	
KCP/CNF-HT	0.66	0.06	19	1.0	
KCP/CNF-0.5OX	0.66	0.06	19	1.0	CNF support oxidized in 0.5 M HNO_3
KCP/CNF-15OX	0.66	0.06	19	1.0	CNF support oxidized in 1:1 mixture of 15 M HNO_3 and 18 M H_2SO_4
C/CNF	0.66	–	–	–	$CuCl_2$ only
CP/CNF	0.66	0.06	19	–	$CuCl_2$ and $PdCl_2$ only

[a] On a wt.% metal basis.
[b] Atomic ratio of Cu/Pd.
[c] Molar ratio of KCl/Cu.

A run was initiated by loading 150 mg of catalyst into the reactor and then heating it to 423 K in 60 cm^3/min of He. The flow of reactants was started immediately upon reaching 423 K. The feed to the reactor contained CO (61%), O_2 (5%), ethanol (13%), and He (24%), which were flowed over the catalyst at a total flow rate of 69 cm^3/min (STP). For stability experiments, CCl_4 (0–104 ppm) was also added to the feed. All reactions were carried out at 3.1 bar. After reaction, catalysts were cooled in He and then stored at ambient conditions. All catalysts were tested for at least 10 h to assess the extent of catalyst deactivation. Measurements of catalytic activity and selectivity could be reproduced within an experimental error of about 5%.

The reaction products were identified and quantified by gas chromatography (Agilent 6890GC) at 45-min intervals. Details of the GC analysis have been presented in Ref. [13]. Because catalyst loadings were adjusted for surface area, and because $CuCl_x$ was the majority component relative to $PdCl_2$, activities were usually normalized to the moles of Cu in the catalyst (mmol product/mol Cu/s). CO_2, acetaldehyde, and 1,1-diethoxyethane (acetal) were the only significant byproducts detected. While water was observed in the reaction products, its concentration was not quantified.

For selectivity calculations, CO_2 was considered to be derived from the oxidation of CO (Eq. (3)). Evidence from other studies of DMC synthesis indicates that CO_2 formation can also occur by hydrolysis of alkyl carbonates (Reaction (4), $\Delta G^0 = -12.2$ kcal/mol) [20], but the overall pathway (Reactions (2) and (4)) is equivalent to CO oxidation for the purposes of calculating selectivity. CO_2 activity was negligible when only ethanol and O_2 were passed over the catalyst, and consequently, direct combustion of ethanol was not considered as a path to CO_2.

Acetaldehyde and acetal were derived from ethanol (Eqs. (5) and (6), respectively). Eq. (7) was used to calculate product selectivities from ethanol or CO. In this equation, n_i is the net moles of ethanol or CO required to make the ith product; r_i is the rate of formation of the ith product; and the summation is over all products. For example, the selectivities from ethanol were calculated with $n_{DEC} = 2$, $n_{acetaldehyde} = 1$, and $n_{acetal} = 3$; and the selectivities from CO were calculated with $n_{DEC} = 1$ and $n_{CO_2} = 1$.

$$2CH_3CH_2OH + CO + \frac{1}{2}O_2 \rightarrow (CH_3CH_2O)_2CO + H_2O \quad (2)$$

$$CO + \frac{1}{2}O_2 \rightarrow CO_2 \quad (3)$$

$$(CH_3CH_2O)_2CO + H_2O \rightarrow 2CH_3CH_2OH + CO_2 \quad (4)$$

$$CH_3CH_2OH + \frac{1}{2}O_2 \rightarrow CH_3CHO + H_2O \quad (5)$$

$$CH_3CHO + 2CH_3CH_2OH \rightarrow (CH_3CH_2O)_2CH_2CH_3 + H_2O \quad (6)$$

$$S_i = \frac{n_i r_i}{\sum_j n_j r_j} \quad (7)$$

2.3. Elemental analysis and determination of the point of zero charge (PZC)

Elemental analyses for Cl (IC); CH (combustion); and O (pyrolysis) were carried out by Galbraith Laboratories. The PZC of the carbon supports, i.e., the pH at which the net surface charge is zero, was determined by the mass titration method [29]. The equilibrium pH was measured after vigorously shaking aqueous suspensions of support in water of increasing carbon/water ratio. A plot of pH versus carbon wt.% reached a plateau between 10 and 20 wt.% carbon, and the pH at the plateau value was taken as the PZC of the carbon.

2.4. Infrared spectroscopy

To acquire infrared spectra, each carbon sample was dried at 383 K and diluted to 0.1 wt.% in dry IR-quality KBr (Fisher). Pellets (1 cm dia.) were formed from 100 mg of the diluted carbon–KBr powder using a hydraulic press held at 8000 psi for 2 min. A reference pellet of 100 mg KBr was also pressed.

Transmission IR spectra were acquired using a Nicolet 750 Magna-IR spectrometer. After installing the pellet in the infrared cell, dry nitrogen was flowed continuously to eliminate most atmospheric interference. Single beam spectra were acquired by collecting 200 scans from 4000 cm^{-1} to 600 cm^{-1} at 2 cm^{-1} resolution. A single beam spectrum I was acquired for each carbon sample (I_{carbon}) and for the pure KBr pellet (I_{KBr}). Single beam spectra of the atmosphere (I_{atm}) and the nitrogen-flushed chamber (I_{N_2}) were also obtained for use in processing the spectra, as described below.

Absorbance spectra of carbon samples (A_{carbon}) were calculated using the spectrum of pure KBr as the background spectrum Eq. (8). Absorbance spectra for the KBr pellet (A_{KBr}) and for the atmosphere (A_{atm}) were calculated using the nitrogen spectrum as background Eqs. (9) and (10).

$$A_{carbon} = -\log\left(\frac{I_{carbon}}{I_{KBr}}\right) \quad (8)$$

$$A_{KBr} = -\log\left(\frac{I_{KBr}}{I_{N_2}}\right) \quad (9)$$

$$A_{atm} = -\log\left(\frac{I_{atm}}{I_{N_2}}\right) \quad (10)$$

$$A_{carbon^*} = (A_{carbon} - k_1 * A_{KBr} - k_2 * A_{atm}) \quad (11)$$

The A_{carbon} spectra were refined further by adjusting factors k_1 and k_2 in Eq. (11) such that a KBr artifact at 1384 cm^{-1} and atmospheric contamination were minimized in A_{carbon^*}. A_{carbon^*} spectra were then baseline corrected (to remove background tilt) and smoothed. Finally, each A_{carbon^*} spectrum was baseline corrected in the region from 1750 cm^{-1} to 750 cm^{-1}, and these spectra were compared on a common absorbance scale to assess the type and relative abundance of oxygen groups present on the different supports.

2.5. Scanning electron microscopy (SEM)

The catalyst surface composition and structure were examined by scanning electron microscopy using a S-4300SE/N (Hitachi, USA) scanning electron microscope equipped with an energy dispersive X-ray spectrometer (EDX). The accelerating voltage of the microscope was 15.0–20.0 kV. Catalyst samples were mounted on carbon tape, and measurements were taken at $\sim 10^{-4}$ Pa. Noran System Six software was used to calculate elemental concentrations from X-ray emission profiles.

2.6. High resolution transmission electron microscopy (HR-TEM)

Images of the catalyst surface at 0.5 Å resolution were obtained with the TEAM 0.5 microscope at the National Center for Electron Microscopy (NCEM). TEM samples were prepared by suspending approximately 1 mg catalyst in 1 mL ethanol, sonicating the solution for 5 min, and then applying a small drop of the ethanol suspension onto holey carbon-coated copper grids (SPI Supplies).

3. Results

3.1. Support characterization

3.1.1. Structure of the carbon (HR-TEM)

HR-TEM was employed to examine the nanoscale structure of the carbon supports. The images in Fig. 1 illustrate the differences

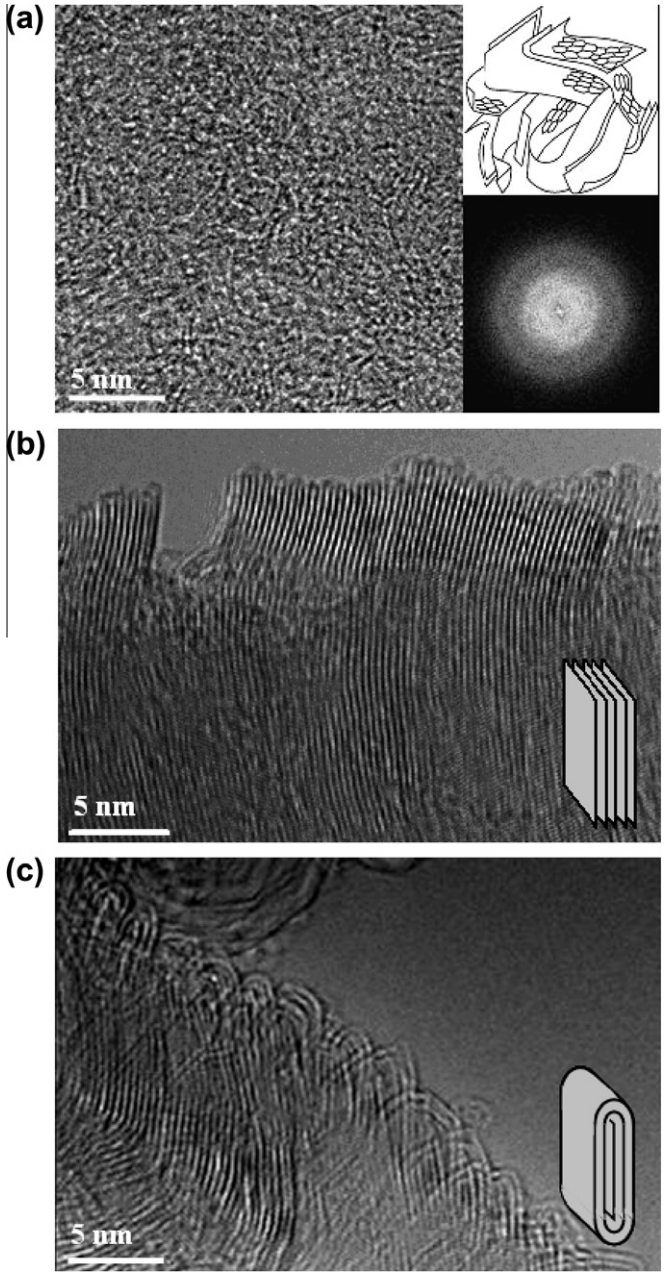

Fig. 1. HR-TEM images of the carbon supports. (a) KCP/AC. Top inset (reproduced by permission from Ref. [64]): a sketch of the turbostratic graphene planes that make up AC; bottom inset: finite Fourier transform (FFT) of the TEM image. (b) KCP/CNF. The cartoon illustrates the "deck of cards" character of platelet-type CNF. (c) KCP/CNF-HT. The cartoon depicts the edge folding that takes place when a platelet-type CNF is subjected to heat treatment.

between KCP/AC (a), KCP/CNF (b), and KCP/CNF-HT (c), all shown after catalyst preparation. The image of AC shown in Fig. 1a is typical for activated carbons. A Fourier transform of this image (bottom inset) reveals rings with spacings characteristic of graphite [30], suggesting that AC is made up of highly disordered graphene layers (top inset).

In contrast to AC, the graphene layers in CNF (Fig. 1b) and CNF-HT (Fig. 1c) are clearly distinguishable. The edges of platelet-type CNF are visible in Fig. 1b, and the inset illustrates the "deck of cards" structure of platelet-like CNF. Fig. 1c illustrates the effect of heat treatment on CNF, which causes the edges to close and bond together, forming envelopes that now expose curved basal planes instead of edge surfaces. The inset gives a simplified illustration of the closed loops formed during heat treatment.

3.1.2. Oxygen content of the carbon supports

The oxygen content of the carbon supports was characterized by three techniques. The PZC of the supports was measured to determine their acidity, and elemental analysis was carried out to measure oxygen content. (The oxygen content of AC could not be analyzed reliably due to interference from silica and alumina impurities.) Finally, the nature and distribution of oxygen-containing functional groups were determined by infrared spectroscopy.

Table 3 lists the PZC and oxygen content for each support. The oxygen content of the CNF-HT support was below the pyrolysis detection limit of 0.5 wt.%. Oxygen content increased progressively in the order CNF < CNF-0.5OX < CNF-15OX, consistent with the trend of increasing acidity observed by PZC analysis. The strongly oxidized CNF-15OX support has significantly higher oxygen content than the other supports, indicating the probable formation of larger O complexes on the surface, including carboxylic acids, lactones, and carbonates.

Characterization of oxygen-containing functional groups by infrared spectroscopy is summarized in Fig. 2. Bands are observed in the regions of 1000–1400 cm^{-1}, characteristic of C—O stretching vibrations in ethers, phenols, esters, lactones, carboxylic acids, and carbonates and to O–H bending modes in phenols; a broad band is observed at 1580 cm^{-1}, due to aromatic C=C stretching vibrations, enhanced by the presence of oxygen-containing functional groups [31]; and bands are also seen in the region of 1660–1750 cm^{-1}, due to C=O stretching vibrations in carboxylic acids, lactones, and other C=O-containing groups [31,32].

The spectrum of AC contains a broad envelope of bands in the region of 900–1300 cm^{-1} due to C—O stretching vibrations from a variety of ethers, alcohols, and phenols. The aromatic C=C contribution at 1580 cm^{-1} is weak because activated carbon has a very disordered carbon structure [32]. This activated carbon appears to have relatively low C=O content, as evidenced by the lack of absorption in the carbonyl stretching region around 1730 cm^{-1}.

Table 3
Summary of the oxygen analysis of the carbon supports used in this study. PZC analysis probes oxidation extent by measuring the relative acidity of the carbons.

Support	PZC	wt.% O
CNF-HT	6.1	<0.5
AC	5.8	–
CNF	2.5	2.3
CNF-0.5OX	–	2.8
CNF-150X	2.2	9.2

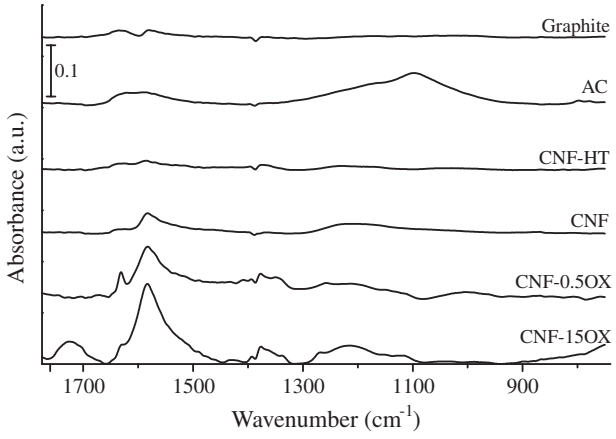

Fig. 2. Transmission IR spectra were collected for the supports used in this study. Each support was diluted to 0.1 wt.% in KBr.

For the carbon nanofiber supports [33], the clearest correlation between the concentration of oxygen and the IR spectrum is exhibited by the intensity of the band at 1580 cm^{-1}, which increases significantly with increasing oxygen concentration. CNF-HT looks remarkably similar to graphite, further establishing the absence of functional groups. CNF exhibits a broad band from 1100 to 1300 cm^{-1}, similar to but weaker than the band in activated carbon. After oxidation, a band between 1300 and 1400 cm^{-1} grows, indicating the possible formation of carbonates, which can exhibit C=O stretching frequencies in the 1590–1600 cm^{-1} region. The formation of carbonyl-containing groups does not occur to an appreciable extent except for the highly oxidized CNF-15OX, which features a strong C=O contribution. Thus, while IR cannot identify the precise nature of the oxygen-containing functional groups that accumulate during oxidation of the CNF support, it is evident that they are associated with the aromatic ring structure, and most likely are located at the edges of the graphene sheets. Strong oxidation is required to achieve significant formation of C=O species.

3.2. Dispersion of catalytic species

The dispersion of catalytic species on the carbon supports was analyzed by SEM. The composition at several points on each catalyst was determined from EDX. While the SEM images for some catalysts exhibited highly dispersed $CuCl_x$ and KCl (as evidenced by a uniform background level of Cu, K and Cl on gray areas of the support), other catalysts featured poorly dispersed KCl and $CuCl_x$ particles. Because of the low loading of $PdCl_2$ on these catalysts and overlap between the Cl K-edge and Pd L-edge X-ray emission lines, Pd species could not be detected by EDX.

Fig. 3 shows representative SEM images of KCP/AC, KCP/CNF, and KCP/CNF-HT at 600× magnification. The nanofibers cluster together to form large, mesoporous particles [23]. Bright spots in these images were identified by EDX as KCl particles ranging from ~100 nm up to several microns in diameter (see areas 1–3 in Fig. 3c). KCl particles are distributed more or less uniformly over the surfaces of KCP/AC and KCP/CNF-HT, but KCP/CNF exhibited far fewer spots, indicating better dispersion of KCl. While the images shown in Fig. 3 show a fraction of the carbon surface, the KCl dispersion they depict is representative of other regions of each catalyst that were examined.

The dispersion of $CuCl_x$ species also depended on the support. Fig. 4a shows an SEM image of KCP/AC. While EDX revealed the presence of dispersed Cu in all regions of the support, crystallites of $CuCl_x$ were also evident, as seen here in region 1. Such crystallites were not observed in the images of KCP/CNF (Fig. 4b), which exhibited a much more uniform distribution of Cu, K, and Cl on the support surface. KCP/CNF-HT (Fig. 4c) showed some areas of uniform dispersion (areas 1–3), but regions of very high Cu and Cl concentration were also found (area 4). The background level of Cu was also higher for KCP/CNF-HT (~1.7) than for KCP/CNF (~0.7), indicating that the Cu penetration into the pores of the support was limited for KCP/CNF-HT relative to KCP/CNF. While not shown, EDX analysis SEM images of KCP/CNF-15OX revealed that the background level of $CuCl_x$ for this catalyst (~0.2) was lower than that for KCP/CNF, indicating higher $CuCl_x$ dispersion.

Additional information about the distribution of Cu and Pd in KCP/CNF were obtained from HR-TEM through-focus images. Heavy elements such as Cu and Pd can be discerned relative to the carbon support, because atoms of these elements appear as bright spots when the electron beam is underfocused and darker spots when the beam is overfocused. The variation in intensity (plotted as percent of maximum contrast (PMC)) with focus can be exploited to identify the element responsible for the bright spot [34]. The expected PMCs (obtained by interpolating between known values for Ge [34] and Au [35]) for Cu and Pd are 13% and 17%, respectively. Fig. 5 shows regions of the KCP/CNF catalyst that are underfocused (a) and overfocused (b), illustrating the variation of intensity with focus for several points. The corresponding analysis is shown in Fig. 5c, which indicates that two of the spots are Pd and the remaining spots are Cu. The intensity of the background carbon (point 1) does not vary with focus. Damage from the electron beam dispersed somewhat larger clusters of heavy (Cu and Pd) atoms that could be observed briefly upon moving the beam to a new region for analysis. Several other HR-TEM through-focus series were acquired to confirm that the Cu and Pd atoms depicted in Fig. 5a are representative of other regions on the CNF surface.

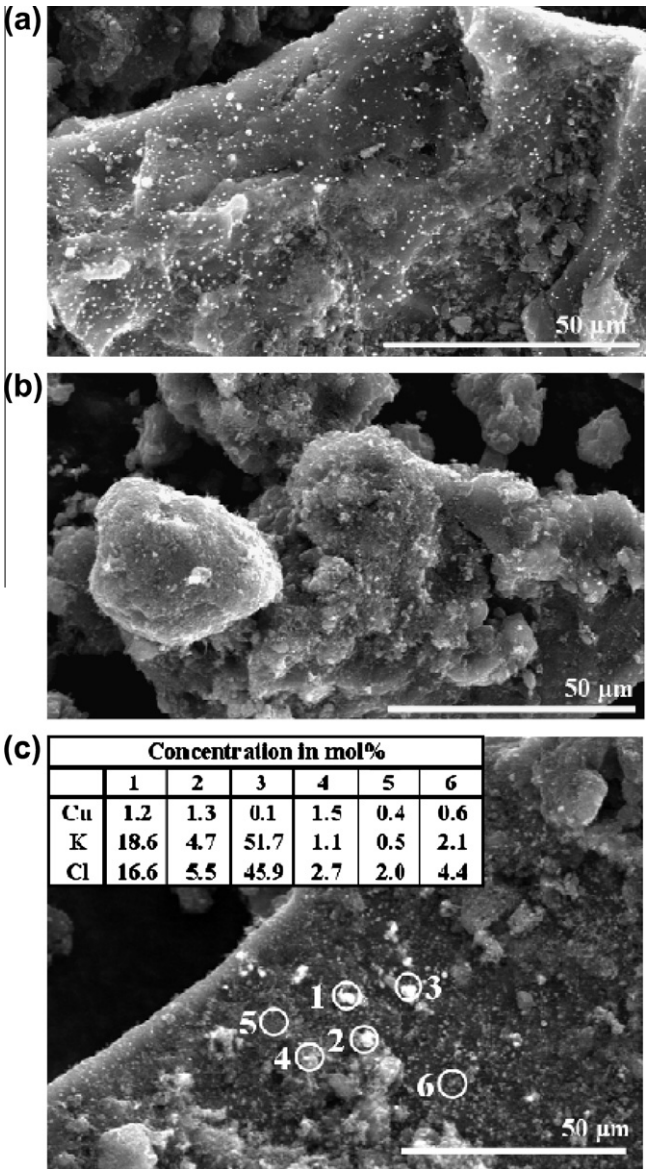

Fig. 3. SEM images (600×) and EDX analyses of KCl dispersion on prepared catalysts. The bright spots in the images are KCl particles identified by EDX: (a) KCP/AC; (b) KCP/CNF; (c) KCP/CNF-HT. The EDX composition at a few points is summarized in the attached table in order to illustrate the variation of KCl content between dark and bright spots.

3.3. Catalysis

3.3.1. Comparison of carbon-supported catalysts

Fig. 6 illustrates the activities and selectivities for catalysts prepared on three different carbon supports: CNF, CNF-HT, and AC.

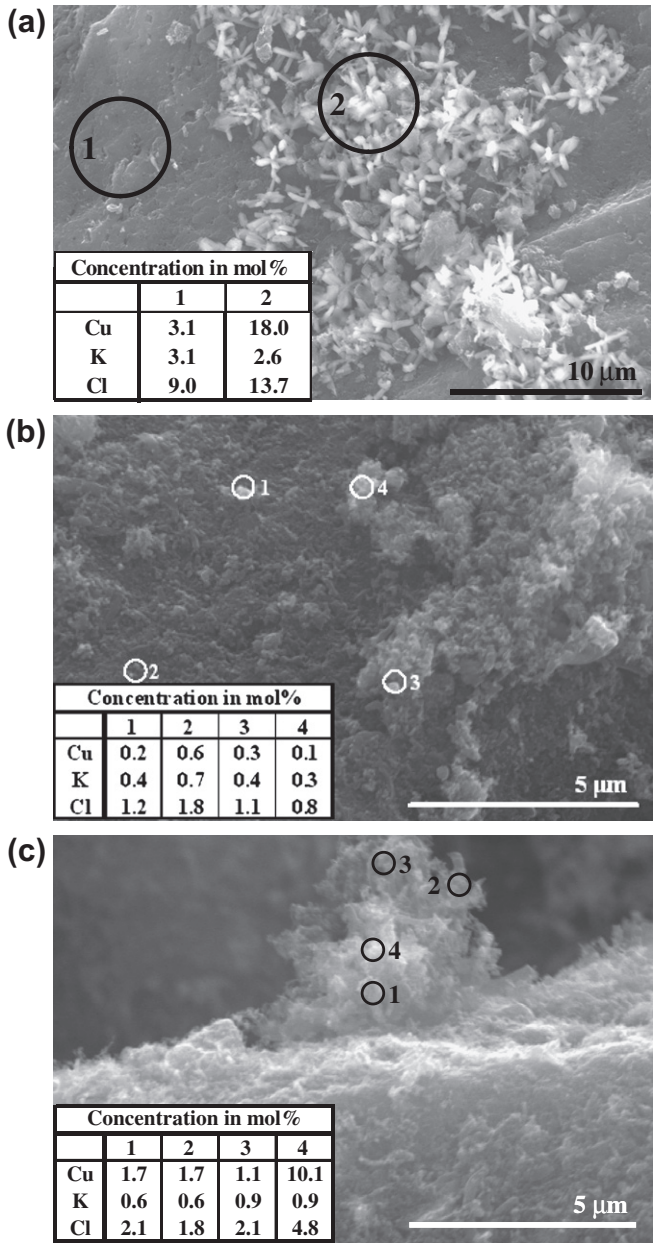

Concentration in mol%

	1	2
Cu	3.1	18.0
K	3.1	2.6
Cl	9.0	13.7

Concentration in mol%

	1	2	3	4
Cu	0.2	0.6	0.3	0.1
K	0.4	0.7	0.4	0.3
Cl	1.2	1.8	1.1	0.8

Concentration in mol%

	1	2	3	4
Cu	1.7	1.7	1.1	10.1
K	0.6	0.6	0.9	0.9
Cl	2.1	1.8	2.1	4.8

Fig. 4. SEM and EDX analyses of $CuCl_x$ species dispersion on: (a) KCP/AC; (b) KCP/CNF; (c) KCP/CNF-HT. The EDX composition at a few points is summarized in the attached tables in order to illustrate the variation of $CuCl_x$ content between dark and bright spots.

The rate of DEC formation based on moles of supported Cu (Fig. 6a) exhibits a similar pattern for all three catalysts – a rise in activity during the first several hours on stream, after which a maximum in activity is reached, and then the activity declines. The maximum activity decreases in the order of KCP/CNF > KCP/CNF-HT > KCP/AC, whereas the rate of activity loss after the maximum is about the same for KCP/CNF and KCP/AC, but significantly higher for KCP/CNF-HT. All three catalysts exhibit a rapid rise in the selectivity to DEC from ethanol (Fig. 6e) to about 92%, after which the selectivity decreases with time in the order KCP/CNF-HT > KCP/AC > KCP/CNF. Interestingly, the DEC selectivity from CO (Fig. 6f) rises rapidly to about 53% and remains relatively constant for KCP/CNF and KCP/AC, but goes through a maximum for KCP/CNF-HT. The activity for the two ethanol-derived byproducts is shown in Fig. 6b (acetaldehyde = open symbols, acetal = filled symbols). The activity for both products based on moles of Cu is virtually the same for all three catalysts and remains nearly constant after a short induction period. Another interesting feature of the results shown in Fig. 6 is that the rate of CO_2 formation rises, reaches a maximum, and then decreases in a manner very similar to that seen for the rate of DEC synthesis, suggesting that the processes for producing DEC and CO_2 are related. A correlation between DEC and CO_2 activity was observed for all of the catalysts tested in this study.

Table 4 compares the maximum activity and selectivity of two of the catalysts investigated in this study with a KCl–NaOH–$CuCl_2$–$PdCl_2$/AC catalyst reported in our previous study [13]. The moles of Cu per square meter of support and the Pd/Cu ratio are nearly the same for all three catalysts, as are the reaction conditions. Comparison of the rates of DEC formation per mole of Cu shows that the activities of the catalysts used in the present study are higher than that reported in Ref. [13], and that the highest rate is observed for KCl–$CuCl_2$–$PdCl_2$/CNF. High DEC activity is attributed to the use of water, rather than methanol, to disperse $CuCl_2$ and $PdCl_2$, and to the use of CNF versus AC as the support.

3.3.2. Effect of KCl and $PdCl_2$

Fig. 7 shows that KCl and especially $PdCl_2$ are required to achieve high activity. $PdCl_2$ is essential to obtaining high DEC activity, an effect observed in previous work on activated carbon supports; however, $PdCl_2$ alone is not active for DEC synthesis [6,7,13]. A further role of $PdCl_2$ is to raise the selectivity to DEC from ethanol by decreasing acetaldehyde and acetal activity, the formation of which are promoted by the dispersed $CuCl_x$ [13]. The addition of KCl prolongs catalyst activity and stabilizes the DEC selectivity from ethanol, but has a negative effect on the DEC selectivity from CO.

3.3.3. Support oxidation

Fig. 8 shows the change in catalyst behavior if CNF is oxidized before adding the catalytically active components. Mild oxidation (KCP/CNF-0.5OX) decreases the activity and selectivity of the catalyst somewhat, whereas strong oxidation (KCP/CNF-15OX) leads to nearly complete loss of DEC activity. It is also evident that oxidation of CNF decreases the selectivities to DEC from both ethanol and CO. As discussed below, a modest amount of CNF oxidation is desirable to disperse the catalytically active component but excessive oxidation is detrimental.

Table 5 compares the DEC activity of each catalyst to a summary of the information obtained from structural characterization. The reported DEC activity was taken after 7 h on stream, at which time each catalyst deactivated at a similar rate. It is apparent that the DEC activity is not a monotonic function of the oxygen content or the PZC, but that there are optima for both metrics. The highest activity was found for CNF, which has a PZC of 2.5 and an oxygen content of 2.3%. CNF exhibited moderate C—O and C=C band intensities and good dispersion of KCl and $CuCl_x$. The lower activities of KCP/AC and KCP/CNF-HT correlate with lower oxygen content and poorer dispersion of KCl and $CuCl_x$. The decrease in activity for KCP/CNF-0.5OX is accompanied by a slight increase in oxygen concentration and increased C=C intensity. Finally, KCP/CNF-15OX displayed very low DEC activity, but exhibited excellent dispersion of KCl and $CuCl_x$. The appearance of C=O functionalities on this highly oxygenated catalyst could be associated with the loss of activity.

3.3.4. CCl_4 concentration

The loss in DEC activity with time on stream for carbon-supported catalysts has been attributed to the gradual loss of Cl [13,36]. Elemental analysis of the KCP/AC catalyst before and after reaction showed that the Cl content dropped from 3.4 wt.% to 1.4 wt.%. Consistent with these observations, several patents report

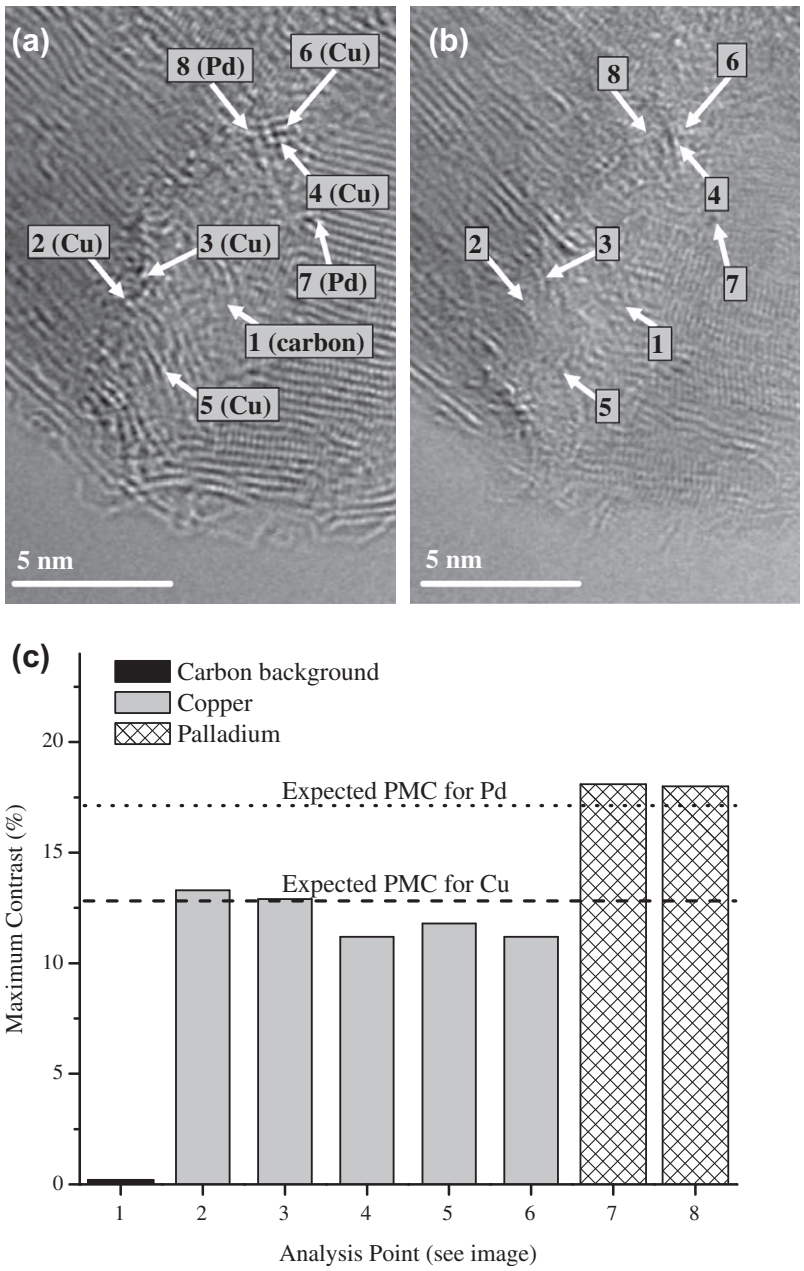

Fig. 5. HR-TEM images of the KCP/CNF catalyst, illustrating the variation of intensity as a function of the focus of the electron beam: (a) at an underfocus of 10.8 nm, Cu and Pd atoms can be distinguished as bright spots; (b) at an overfocus of 3.6 nm, the spot contrast has decreased significantly; and (c) the maximum contrast for each spot.

that catalysts used for dialkyl carbonate synthesis can be regenerated by offline treatment with HCl or other chlorine-containing gases [4,5]. It has also been reported that addition of 0.5 wt.% CCl_4 to the feed resulted in continuous regeneration of alumina-supported $(Et_4N)Cu_4OCl_{10}$ [16], but continuous regeneration of $CuCl_2$/AC was unsuccessful [4]. Stimulated by these results, we explored the addition of very low concentrations of CCl_4 to the feed stream.

Fig. 9 shows the effect of CCl_4 on the DEC activity and selectivity for KCP/AC. For 27 ppm CCl_4, the activity was stabilized significantly but still decreased slowly with time. When the concentration of CCl_4 was raised to 104 ppm, catalyst activity decreased further but now the activity and DEC selectivity became stable. Higher concentrations of CCl_4 (>1000 ppm), however, resulted in very low activity (results not shown).

The effect of adding CCl_4 to CNF-supported catalysts is reported in Fig. 10. Very low concentrations of CCl_4 were sufficient to stabilize the activity of these catalysts. KCP/CNF stabilized at ~3.5 mmol DEC/mol Cu/s after 40 h on stream. KCP/CNF-0.5OX was tested over a range of CCl_4 concentrations (starting at 27 ppm and decreasing the concentration to 2.7 ppm after 20 h). Higher levels of CCl_4 were associated with lower DEC activity and selectivities, so it is desirable to operate at the lowest CCl_4 concentration in order to sustain activity. To confirm that CCl_4 replenished the Cl on the catalyst, the KCP/CNF-0.5OX sample was tested before and after reaction. Cl dropped slightly from 0.9% to 0.8%.

3.3.5. Analysis of CO_2 activity

The selectivity to DEC from CO is limited by significant CO_2 formation. The previously mentioned correlation between DEC and CO_2 activity suggests that CO_2 activity originates from a process related to DEC synthesis. This could be explained by a series pathway involving decomposition from DEC to CO_2, or by a parallel pathway that competes with DEC for the same active sites. An attempt to

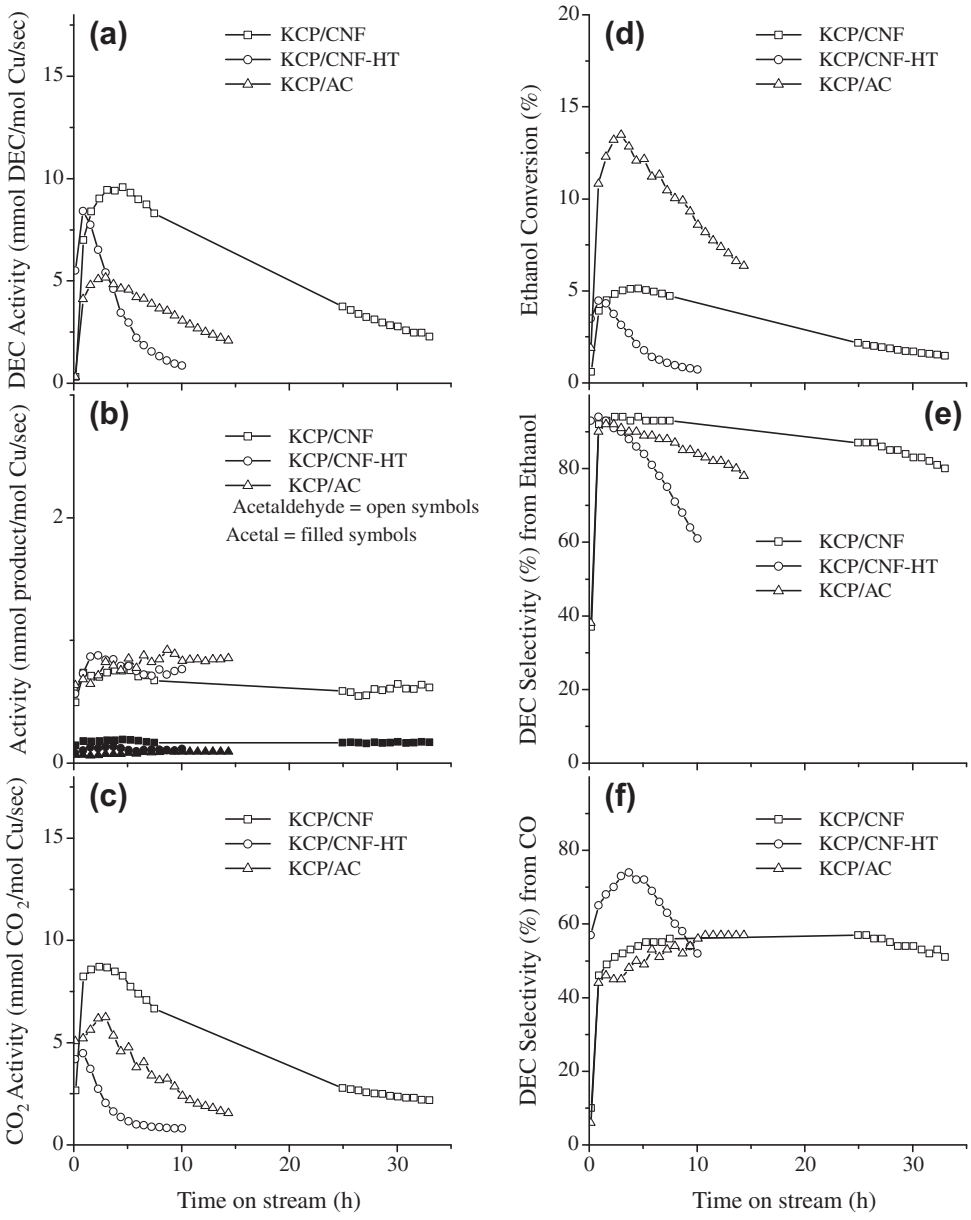

Fig. 6. The effect of carbon support on activity for KCP/CNF, KCP/CNF-HT, KCP/AC. (a–c): Rate of DEC, acetaldehyde, and CO_2 formation per mole of Cu; (d): ethanol conversion; (e–f): DEC selectivities from ethanol and CO. Reaction conditions: T = 423 K, P = 3.1 bar, $CO/O_2/EtOH$ = 61/5/13, Q = 69 cm^3/min (STP), catalyst = 150 mg. Catalyst compositions are shown in Table 2.

Table 4
Comparison of the activity, ethanol conversion, and ethanol selectivity of carbon-supported catalysts used for DEC synthesis.

Catalyst	Rate[a]	Conversion[b] (%)	Selectivity[c] (%)
KCl–NaOH–$CuCl_2$–$PdCl_2$/AC (Ref. [13])	3.7	6	90
KCl–$CuCl_2$–$PdCl_2$/AC (this work)	5.2	13	91
KCl–$CuCl_2$–$PdCl_2$/CNF (this work)	9.6	5	94

[a] mmol DEC/mol Cu-s.
[b] Total conversion of ethanol.
[c] Selectivity to DEC from ethanol.

diagnose the source of CO_2 activity was carried out by varying the reaction conditions for the KCP/AC catalyst. Because H_2O is produced as a byproduct of DEC synthesis (Reaction (2)) and is known to participate in the oxidation of CO [37], the effect of introducing additional H_2O to the feed gases was examined.

CCl_4 was added to the reactants in order to stabilize the catalyst and allow comparison of activities measured at different times. Table 6 shows the results of this investigation. Under regular DEC synthesis conditions (entry 1), the CO_2 activity was 7.8 mmol CO_2/mol Cu/s. The addition of 0.7 mol% H_2O to the feed (entry 2) led to a 58% increase in CO_2 activity, confirming that H_2O plays a role in catalyzing CO_2 synthesis. Entry 3 shows that when CO and O_2 were passed over the catalyst, the rate of CO_2 formation decreased gradually over a 10-h period until only a trace of activity remained. Finally, the addition of 0.7 mol% H_2O (an amount similar to that produced during DEC synthesis) to the CO/O_2 feed (entry 4) resulted in restoration of the CO_2 activity to levels similar to those observed during DEC synthesis (entry 1).

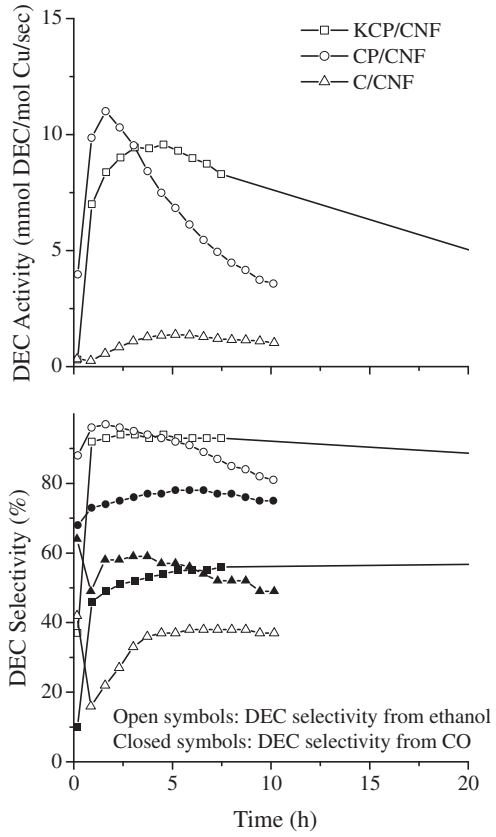

Fig. 7. The effects of KCl and $PdCl_2$ on KCP/CNF activity and selectivity of CNF-supported catalysts. Selectivities to DEC from ethanol (open symbols) and CO (closed symbols) are also shown. Reaction conditions are identical to those in Fig. 6, and catalyst compositions are in Table 2.

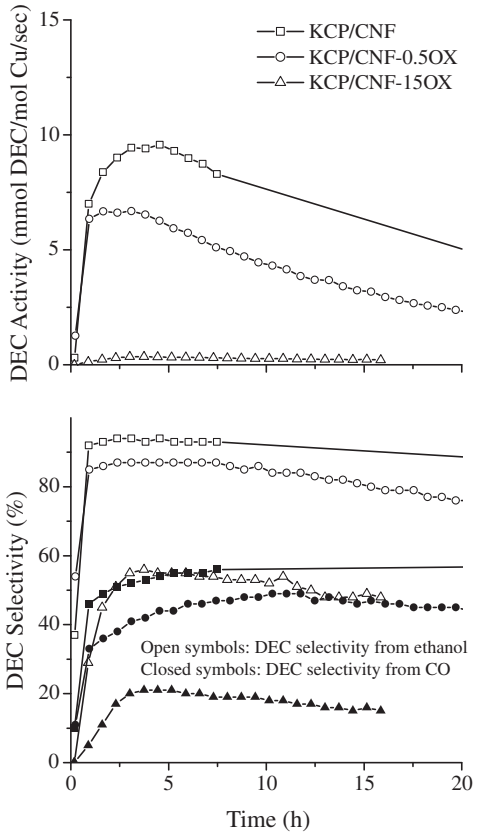

Fig. 8. Effects of oxidizing the CNF support prior to catalyst preparation on catalyst activity and selectivity. DEC activity is normalized by moles of Cu. Selectivities to DEC from ethanol (open symbols) and CO (closed symbols) are also shown. Reaction conditions are identical to those in Fig. 6, and catalyst compositions are in Table 2.

4. Discussion

The results presented in the preceding section demonstrate that the catalysts used in this study are complex and that their activity and selectivity for DEC synthesis are strongly dependent on the structure and pretreatment of the support and on the dispersion of the two principal components from which the catalytically active species are formed, $CuCl_2$ and $PdCl_2$. To develop an understanding of the composition and structure of the active species involved in DEC synthesis, it is necessary to consider the structure of the support and the extent of its oxidation, the manner in which the catalyst precursors interact with the support during catalyst preparation, and the final state of these components after the catalyst has been placed under reaction conditions. These issues will be examined in Sections 4.1–4.3. In Section 4.4, the overall structure of the catalyst, as developed in Sections 4.1–4.3, is used to interpret the roles of $CuCl_x$, $PdCl_2$, KCl, and CCl_4 in the synthesis of DEC on carbon-supported catalysts. This discussion is followed by a proposal for the mechanism of DEC formation and for the processes by which CO_2 is formed.

4.1. Structure of the carbon support

The structure of both AC and CNF is based on the stacking of graphene layers [21,23]. AC consists of curved graphene sheets that are turbostratic, i.e., disordered with respect to each other, whereas CNF consists of highly ordered graphene sheets. The TEM micrographs shown in Fig. 1 are fully consistent with this description. The absence of any structural order in the image of AC is characteristic of the irregular structure of the material; however, the Fourier transform of this image does reveal rings that have a spacing consistent with those of graphite. The sketch associated with the image shown in Fig. 1a gives a view of the highly disordered nature of AC. By contrast, the image of acid-washed CNF shows regularly stacked graphene sheets with interplanar distances of 0.34 nm, characteristic of lamellar graphite. Fig. 1c shows that, upon heat treatment, the edges of the graphene sheets react to form a continuous, or nearly continuous sheet.

Both AC and CNF exhibit two types of sites – those located at the edges of the graphene sheets and those located on the basal planes. The reactivity of carbon supports with regard to oxidation is strongly dependent on the type of sites exposed. Sites on the basal planes are much less reactive towards oxygen than those at the edges of the graphene sheets [38]. Other variations in the structure of carbons include the presence of defects (e.g. vacancies in the carbon structure and saturated carbon bonds) or turbostratic (i.e. bent and disordered) graphene layers. The reactivity of carbon surfaces decreases in the order (defects) > (edges) > (basal planes) [39]. Based on these considerations, the relative susceptibility of the supports to oxidation increases in the order CNF-HT < AC < CNF.

Oxidation of carbon supports produces a variety of functional groups such as those illustrated in Fig. 11 [39]. Mild oxidation leads to the formation of etheric and phenolic oxygen, whereas carboxylic groups and anhydrides, as well as other forms of C=O groups, appear after more extensive oxidation [22,33]. PZC measurements and elemental analysis (Table 3) showed that the oxygen content of the carbon supports used in this study increased in the order CNF-HT < AC < CNF < CNF-0.5OX < CNF-15OX. IR spectroscopy (Fig. 2) provides further distinctions among the types of oxygen groups present on each support. CNF-HT and CNF-15OX repre-

Table 5
Relationship of DEC activity with the structural characteristics of each catalyst.

Support	DEC activity[a] after 7 h	PZC	wt.% 0	Infrared band intensity			Dispersion[b]	
				C—O	O-modified C=C	C=O	KC1	$CuCl_x$
CNF-HT	1.9	6.1	<0.5	V. weak	V. weak	None	Poor	Poor
AC	4.1	5.8	–	Strong	Weak	None	Poor	Poor
CNF	8.7	2.5	2.3	Moderate	Moderate	None	Good	Good
CNF-0.5OX	5.4		2.8	Moderate	Strong	None	–	–
CNF-150X	0.3	2.2	9.2	Moderate	V. strong	Strong	V. good	V. good

[a] mmol DEC/mol Cu/s.
[b] Dispersion of the components shown was obtained by SEM.

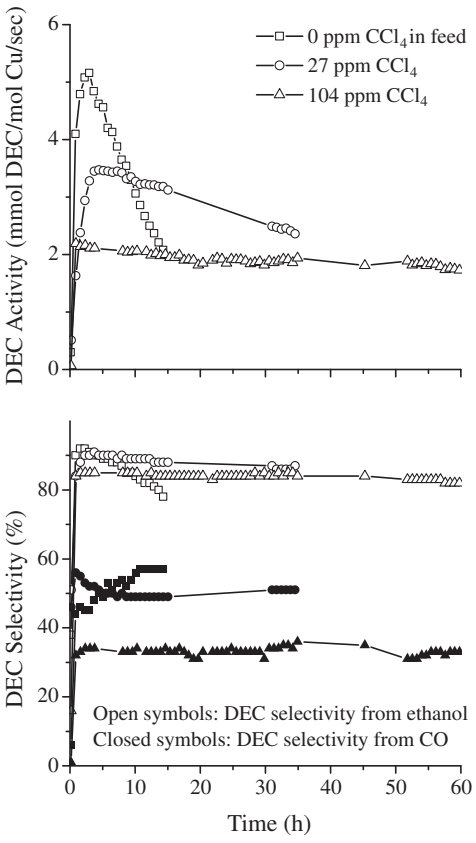

Fig. 9. The effect of adding CCl_4 to the feed stream on the activity and selectivity of KCP/AC (Table 2). Activity to DEC is normalized by moles of Cu. Selectivities to DEC from ethanol (open symbols) and CO (closed symbols) are also shown. Reaction conditions are identical to those in Fig. 6, except where addition of CCl_4 to the feed is noted.

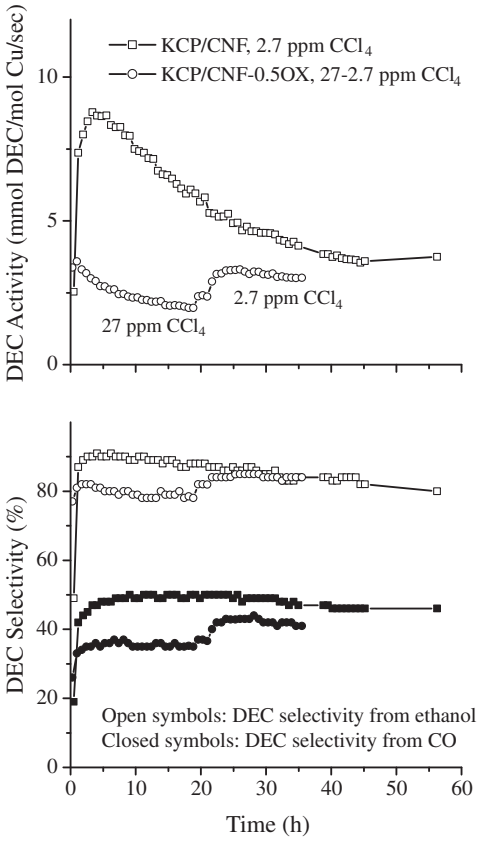

Fig. 10. The effect of adding CCl_4 to the feed stream on the activity and selectivity of KCP/CNF and KCP/CNF-0.5OX (Table 2). Activity to DEC is normalized by moles of Cu. Selectivities to DEC from ethanol (open symbols) and CO (closed symbols) are also shown. Reaction conditions are identical to those in Fig. 6, except the addition of CCl_4 to the feed. KCP/CNF was tested with 2.7 ppm CCl_4, and the last point at 56 h was taken at slightly elevated pressure, 3.3 bar. KCP/CNF-0.5OX was tested over a range of CCl_4 concentration, starting at 27 ppm and decreasing to 2.7 ppm CCl_4 after 20 h.

sented extremes in oxygen content. Oxygen could not be detected by elemental analysis on CNF-HT, and its IR spectrum resembles that of graphite. By contrast, elemental analysis shows that CNF-15OX has an oxygen content of 9.2%. All other supports exhibited only C—O functionalities (ethers and phenols), while the CNF-15OX support exhibited a strong C=O band, suggesting the presence of carbonyls, carboxylic acids, lactones, and anhydrides.

4.2. Interaction between catalyst precursors and the carbon support

The catalysts used in this study were prepared by incipient wetness impregnation of the carbon supports with an aqueous solution of $CuCl_2$, $PdCl_2$, and KCl. The dominant species present in this solution can be inferred from previous studies of similar systems. KCl dissolves readily to form K^+ and Cl^-. Because of the high Cl/Pd ratio, ~22, $[PdCl_4]^{2-}$ anions are expected to be the dominant Pd species in solution [25,26,40]. At ambient temperature and Cl/Cu ~ 2, $CuCl_2$ is expected to form $[Cu(H_2O)_6]^{2+}$ complexes and Cl^- [41,42].

The interactions of the precursor solution with the carbon support are key to preparing an active catalyst. While little is known about such interactions for $CuCl_2$ solutions, the interactions of $PdCl_2$ solutions with carbon have been studied extensively, and these can be used to gain some insight into the types of interactions that $CuCl_2$ may undergo with the support [25,26].

The interaction of $PdCl_4^{2-}$ with carbon involves two competing processes [26,40]: (1) reduction of $[PdCl_4]^{2-}$ to Pd^0 (Reaction (12)), accompanied by the creation of so-called C^+ and (2) dispersion of $PdCl_2$ species on the carbon surface (Reaction (13)).

Table 6
Effect of CO, O_2, and H_2O on the steady-state CO_2 activity for KCP/AC. In addition to the gases listed in the table, 104 ppm CCl_4 was added to the feed stream in order to maintain catalyst activity. DEC synthesis produces H_2O as a byproduct Eq. (2). y_i is the mole fraction of component i in the feed.

Condition	Reactants	CO_2 activity (mmol CO_2/mol Cu/s)	Reactant concentrations (feed values)			
			y_{O_2}	Y_{H_2O}	y_{CO}	y_{EtOH}
1	$CO/EtOH/O_2$	7.8	0.053	0	0.42	0.13
2	$CO/EtOH/O_2/H_2O$	12.3	0.053	0.007	0.42	0.10
3	CO/O_2	0.5	0.053	0	0.42	0
4	$CO/O_2/H_2O$	8.4	0.053	0.007	0.42	0

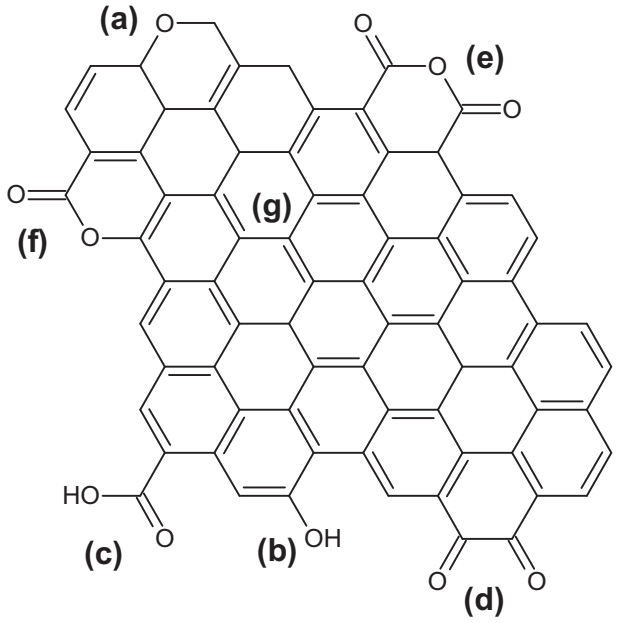

Fig. 11. Illustration of oxygen-containing groups on a carbon support: (a) ether, (b) phenol, (c) carboxylic acid, (d) quinone, (e) carboxylic anhydride, (f) lactone, and (g) aromatic network constituting the basal plane of carbons.

$$C + [PdCl_4]^{2-} \rightarrow Pd^0/C + 2Cl^-/C^+ + 2Cl^- \quad (12)$$

$$C + [PdCl_4]^{2-} \rightarrow PdCl_2/C + 2Cl^- \quad (13)$$

The reducing power of carbonaceous materials is well known and has been attributed to electrons derived from carbon oxidation (Reaction (14)) that then move to the surface of the support where they can reduce adsorbed species (Reaction (15)) [40].

$$C + H_2O \rightarrow CO + 2H^+ + 2e^- \quad (14)$$

$$[PdCl_4]^{2-} + 2e^- \rightarrow Pd + 4Cl^- \quad (15)$$

The formation of metallic Pd is minimized, though, when $PdCl_2$ is introduced by incipient wetness in the presence of excess chloride anions onto partially oxidized carbon, the conditions used in the present study [25]. Thus, consistent with the observation of our previous work [13] and those of the present investigation, only $PdCl_2$ is present on the catalyst surface after incipient wetness impregnation. The dispersion of $PdCl_2$, though, is highly dependent on the structure and pretreatment of the surface. On AC, drying produces $PdCl_2$ crystallites [13] (30 nm), whereas on all acid-treated CNF, $PdCl_2$ is near-atomically dispersed.

Interactions between $[Cu(H_2O)_6]^{2+}$ and the support are presumed to follow similar pathways to $PdCl_2$. $[Cu(H_2O)_6]^{2+}$ complexes can react with Cl^- to form $[CuCl_2]^-$ in the presence of a reductant [42], in this case using electrons from the carbon support (Reaction (16)). The conditions for $PdCl_2$ dispersion should also favor the dispersion of $[CuCl_2]^-$ complexes.

$$[Cu(H_2O)_6]^{2+} + 2Cl^- + e^- \rightarrow [CuCl_2]^- + 6H_2O \quad (16)$$

As in the case of $PdCl_2$, the dispersion of the Cu is highly dependent on the structure and pretreatment of the support. Upon drying, crystallites of $CuCl_2$ were observed on AC [13], but on acid-treated CNF, the Cu species are near-atomically dispersed.

During incipient wetness impregnation, the precursor solution infiltrates the pores of the support and the aqueous solvent evaporates almost immediately. Assuming that K^+, Cl^-, $[CuCl_2]^-$, and $[PdCl_4]^{2-}$ are the dominant species after interaction with the carbon support, the removal of solvent likely leads to the formation of KCl, $[CuCl_2]^-/C^+$, $PdCl_2$, and $[PdCl_4]^{2-}/2C^+$. Some Cl^- may also be adsorbed to the surface of the carbon [25]. A wide variety of chlorocuprates(I) could be formed as the solvent evaporated from the support [43]. Finally, potassium chlorocuprates such as K_2CuCl_3 may also form (Reaction (17)) [44].

$$2K^+ + [CuCl_2]^- + Cl^- \rightarrow K_2CuCl_3 \quad (17)$$

The dispersion of the impregnated species is correlated strongly with the oxygen content of the support. SEM images (Figs. 3 and 4) showed progressively higher dispersion of K, Cu, and Cl in the order CNF-HT ~ AC ≪ CNF < CNF-15OX. The literature on carbon supports has shown that support oxidation can affect the dispersion of salts in several ways [22,26]: (1) by increasing the hydrophilicity of the nominally hydrophobic carbon support, thereby facilitating passage of precursor ions throughout the pores of the support; (2) by altering the electronic properties of the carbon, thereby changing the catalyst–support interaction; and (3) by attracting and anchoring catalyst precursors to the support. All three of these effects are likely to contribute to the high dispersion observed on the oxygen-containing catalysts in this study. The relatively hydrophobic nature of CNF-HT and AC supports very likely hindered full penetration of the aqueous solution of the catalyst precursors into the micropores of the support, resulting in the formation of larger KCl and $CuCl_2$ clusters seen in the SEM images. While the effects of oxidation of carbon supports on the dispersion of $CuCl_2$ have not been reported, several investigators have noted that oxidation of such supports creates acidic centers that favor high dispersion of $PdCl_2$, as well as other metal precursors [25,26,40,45,46].

4.3. Structure of the active species and their interactions with the support

It is evident from Fig. 7 that both $CuCl_2$ and $PdCl_2$ are necessary to achieve high DEC activity and selectivity. While $CuCl_2$ can catalyze the reaction, it is less active than when present with $PdCl_2$ and the selectivity to DEC is lower. The level of Cl in the catalyst must be maintained, since Cl loss leads to a progressive decrease in DEC synthesis activity, a trend that can be offset by continuous addition of CCl_4 to the feed (see Figs. 9 and 10). These observations lead to the hypothesis that the catalytically active species involved in DEC formation contain Cu, Pd, and Cl, in full agreement with the conclusions of previous authors [13,47,48].

Small $CuCl_x$ clusters have a structure similar to that bulk $CuCl_2$ [49], in which linear chains of Cu are bridged by Cl, and are shown

to be active for oxidation and oxidative carbonylation [16,50–53]. Bulk $PdCl_2$ has a structure similar to $CuCl_2$ [54], and it has been shown that Pd^{2+} cations can substitute into $CuCl_2$ clusters to form Cu–Cl–Pd bridging structures [55,56]. Based on these considerations, we propose that the high DEC activity of carbon-supported catalysts is due to the formation of Cu–Cl–Pd complexes. The presence of such complexes can only be suggested, since direct evidence for their presence could not be obtained. Fig. 5 provides some indication that Cu and Pd are proximate to each other (see points 4 and 8). It is hard to tell, though, whether additional Cu–Pd aggregates were present prior to exposure of the sample to the electron beam of the HR-TEM, since such structures can be damaged by the beam. Fig. 12 illustrates how Cu–Cl–Pd complexes could be stabilized at the edges of graphene sheets by means of dative bonding to oxygen-containing species. Since the ratio of Cu/Pd is 20, a significant fraction of the Cu in the catalyst likely exists as $M^+[CuCl_2]^-$ or Cu_nCl_n species, where M^+ could be K^+ or C^+ (deficiencies in carbon electronic structure, see Section 4.2). We have shown that KCl extends the lifetime of the catalyst and contributes to the high Cl/Pd ratio during preparation (see Section 4.2), which inhibits the formation of Pd^0. As discussed above, K^+ may also form potassium chlorocuprate compounds that stabilize active Cu species. Some of the proposed complexes described above are illustrated in Fig. 12.

To summarize, carbon supports for DEC synthesis must contain an intermediate level of oxygen coverage in the form of phenols and ethers. These oxygen functionalities enhance wetting of the surface during catalyst preparation and promote the adsorption of $PdCl_2$ and $CuCl_x$ species on the support. The catalytically active species are thought to consist of complexes with Cl bridging Cu and Pd atoms formed by the reaction of Pd^{2+} cations with $[CuCl_2]^-$ anions.

4.4. Proposed reaction mechanism

4.4.1. Role of $CuCl_2$

Fig. 7 shows that DEC can be formed when $CuCl_2$ is supported in the absence of $PdCl_2$.

A mechanism for the oxidative carbonylation of alcohols to form dialkyl carbonates using a $CuCl_2$ slurry has been proposed [57], and a number of authors have suggested that a similar mechanism is operative for carbon-supported $CuCl_2$ catalysts [13,17,20,36,58–60]. An important feature of this mechanism is the reduction of Cu^{2+} to Cu^+ species. The presence of CuCl is thought to be essential for the activation of ethanol in the first step of the reaction sequence. As shown in Eq. (18), cuprous chloride is re-oxidized upon reaction with ethanol and molecular oxygen to form an ethoxide species and releases water. While Cu(I) species can perform this chemistry readily, it does not occur for Cu(II) species [17,51]. The insertion of CO to form carboethoxide species may occur directly from the gas phase [17,59] (Reaction (19)) or by adsorption (Reaction (20)) and transfer (Reaction (21)) from an adjacent Cu species in accordance with the homogeneous mechanism [57,60]. Finally, the carboethoxide species react with ethoxide species to produce DEC, and the two catalytic sites are regenerated (Reaction (22)).

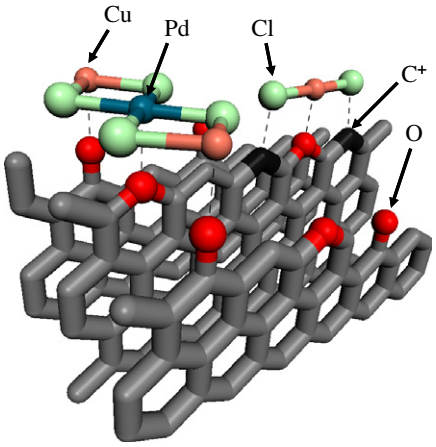

Fig. 12. Proposed bonding of $[CuCl_2]^-Pd^{2+}[CuCl_2]^-$ and $[CuCl_2]^-$ to the support, via oxygen attached to the support surface. C^+ represents electron deficiencies in the graphene network, as discussed above. Dashed lines indicate dative bonding interactions with the support.

$$2CuCl + 2EtOH + 1/2O_2 \rightarrow 2Cu(OEt)Cl + H_2O \quad (18)$$

$$Cu(OEt)Cl + CO \rightarrow Cu(COOEt)Cl \quad (19)$$

$$CuCl + CO \rightarrow Cu(CO)Cl \quad (20)$$

$$Cu(OEt)Cl + Cu(CO)Cl \rightarrow Cu(COOEt)Cl + CuCl \quad (21)$$

$$Cu(COOEt)Cl + Cu(OEt)Cl \rightarrow 2CuCl + (OEt)_2CO \quad (22)$$

4.4.2. Role of $PdCl_2$

$PdCl_2$ does not catalyze DEC synthesis independently of $CuCl_2$ (see Fig. 7 and Ref. [13]). However, it is known that $PdCl_2$ will promote the oxidative carbonylation of alcohols in the presence of a co-oxidant such as LiCl, $CuCl_2$, $FeCl_3$, and I^- [47,61–63]. The latter species are required to form ethoxide species via a process analogous to Reaction (18). Therefore, it is thought that the role of $PdCl_2$ must be to accelerate the formation of carboethoxide species. This idea is supported by the observation that $PdCl_2$ will form carboethoxides (in the presence of a base to form the ethoxides) [62]. The overall process is summarized in Reaction (23), where B = base (such as those listed above) and R = alkyl.

$$PdCl_2 + CO + B \xrightarrow{ROH,-BH^+,-X^-} PdCl(CO)OR \quad (23)$$

Following this logic, we propose that the combination of $PdCl_2$ and CuCl facilitates the formation of carboethoxide species and the subsequent formation of DEC.

Reactions (24)–(28) present a proposal for the manner in which Pd and Cu may be involved in the formation of DEC. Since Pd and Cu are bridged through Cl, coordinated species can be shared easily, and the charge distribution on the overall complex can adjust according to the requirements of each step. Cu forms the ethoxide (Reaction (24)), Pd adsorbs CO (Reaction (25)), and then an ethoxide migrates to the CO coordinated to the Pd^{2+} cation to form the carboethoxide species (Reaction (26)). This step, which is thought to be rate-limiting, should proceed more readily on Pd^{2+} than Cu^+, since the carbonyl group associated with Pd^{2+} should be a stronger electrophile. The carboethoxide species then reacts with ethoxide species to form DEC, and the original Cl coordination of the precursors is restored (Reactions (27) and (28)). The observation that a large excess of $CuCl_2$ to $PdCl_2$ optimizes the activity suggests that Reactions (26) and (27) occur slowly relative to other parts of the mechanism, establishing a need for excess ethoxide.

$$2CuCl + 2EtOH + 1/2O_2 \rightarrow 2Cu(OEt)Cl + H_2O \quad (24)$$

$$PdCl_2 + CO \rightarrow Pd(CO)Cl_2 \quad (25)$$

$$Cu(OEt)Cl + Pd(CO)Cl_2 \rightarrow Pd(COOEt)Cl + CuCl_2 \quad (26)$$

$$Pd(COOEt)Cl + Cu(OEt)Cl \rightarrow Pd(OEt)(COOEt) + CuCl_2 \quad (27)$$

$$Pd(OEt)(COOEt) + 2CuCl_2 \rightarrow PdCl_2 + 2CuCl + (OEt)_2CO \quad (28)$$

4.4.3. Role of Cl and catalyst stability

Cl must be retained on KCP/carbon catalysts to maintain their activity. A similar observation has been made for oxidative carbonylation of alcohols carried out in $CuCl_2$ suspensions [57]. The loss of chlorine from heterogeneous catalysts can be explained by the slow formation of ethyl chloride (Reaction (29)) and paratacamite, $Cu_2Cl(OH)_3$, both of which have been observed in studies of gas-phase synthesis of DEC [13,36].

$$2CuCl + 1/2O_2 + H_2O + C_2H_5OH \rightarrow Cu_2Cl(OH)_3 + C_2H_5Cl \quad (29)$$

Catalyst activity and selectivity to DEC can be maintained by the addition of ppm levels of CCl_4 to the feed; however, high feed concentrations of CCl_4 reduce catalytic activity. CCl_4 is needed to restore Cl-depleted species, whereas excess CCl_4 may lead to the conversion of CuCl to catalytically inactive $CuCl_2$.

4.4.4. Formation of CO_2

Several processes can be envisioned by which CO_2 can be formed. The first is the oxidation of CO. As shown in Table 5, this reaction can be ruled out, since the concentration of CO_2 observed for this reaction is an order of magnitude lower than that observed during DEC synthesis. The oxidation of ethanol was investigated, but this reaction was also found to be slow [13]. The decomposition of DEC via the reaction

$$(CH_3O)_2CO + H_2O \rightarrow 2C_2H_5OH + CO_2 \quad (30)$$

is thermodynamically favorable but is too slow to be the major source of CO_2, as may be inferred from a study of DEC decomposition on Cu^+-zeolites [60]. The results presented in Table 6 suggest that CO_2 is formed by the reaction of CO with the H_2O produced as a coproduct of DEC synthesis via the water–gas-shift reaction. The H_2 produced by this reaction is then combusted, so that the net reaction, as shown by Reactions (31) and (32), is the oxidation of CO to CO_2.

$$CO + H_2O \rightarrow CO_2 + H_2 \quad (31)$$

$$H_2 + 0.5O_2 \rightarrow H_2O \quad (32)$$

5. Conclusion

This study has shown that the activity and selectivity of carbon-supported chlorides of Cu and Pd are strongly dependent on the structure and pretreatment of the support. Highest DEC activity was achieved with acid-pretreated CNF, whereas the lowest activity was found for catalysts supported on AC and heat-treated CNF. Catalyst activity was enhanced by a high proportion of edge versus basal sites on the graphene sheets comprising the support and a modest degree of edge-site oxidation. Maintenance of catalyst activity was achieved by continuous addition of low concentrations of CCl_4 (ppm level) to the feed. Characterization of the catalysts by SEM and TEM revealed that the Cu and Pd on acid-treated CNF are near-atomically dispersed. Based on the results of this investigation and earlier work, it is proposed that the active sites for DEC synthesis consist of $Pd[CuCl_2]_2$ species stabilized by dative bonding with oxygen-containing species present at the edges of graphene sheets comprising the support. A mechanism for the formation of DEC is proposed, in which CuCl species adsorb ethanol dissociatively to form ethoxide species, and Pd^{2+} cations adsorb CO. Migration of ethoxide species to the adsorbed CO results in the formation of carboethoxide species, which then react with an additional ethoxide species to form DEC. While DEC can be formed in the absence of Pd^{2+}, CO adsorbed on Pd^{2+} is more electrophilic than CO adsorbed on Cu^+, and, hence, more reactive towards the addition of ethoxide species, the process that is thought to be rate-limiting.

Acknowledgments

The authors acknowledge support from the National Center for Electron Microscopy, Lawrence Berkeley National Laboratory, which is supported by the US Department of Energy, under Contract No. DE-AC02-05CH11231.We gratefully acknowledge Christian Kisielowski and Chengyu Song for their assistance in the collection and analysis of HR-TEM data. This work was supported by the Methane Conversion Cooperative (MC^2) funded by BP.

References

[1] M.A. Pacheco, C.L. Marshall, Energy Fuels 11 (1997) 2–29.
[2] A.-A.G. Shaikh, S. Sivaram, Chem. Rev. 96 (1996) 951–976.
[3] U. Romano, R. Tesei, G. Cipriani, L. Micucci, US Patent 4,218,391, 1980.
[4] G. L. Curnutt, US Patent 5,004,827, 1991.
[5] T. Koyama, M. Tonosaki, N. Yamada, K. Mori, US Patent 5,650,369, 1997.
[6] Y.J. Wang, Y.Q. Zhao, B.G. Yuan, B.C. Zhang, J.S. Cong, Appl. Catal. A 171 (1998) 255–260.
[7] B.C. Dunn, C. Guenneau, S.A. Hilton, J. Pahnke, E.M. Eyring, Energy Fuels 16 (2002) 177–181.
[8] A. Punnoose, M.S. Seehra, B.C. Dunn, E.M. Eyring, Energy Fuels 16 (2002) 182–188.
[9] R.X. Jiang, Y.J. Wang, X.Q. Zhao, S.F. Wang, C.Q. Jin, C.F. Zhang, J. Mol. Catal. A: Chem. 185 (2002) 159–166.
[10] P. Yang, Y. Cao, W.-L. Dai, J.-F. Deng, K.-N. Fan, Appl. Catal. A 243 (2003) 323–331.
[11] H. Itoh, Y. Watanabe, K. Mori, H. Umino, Green Chem. 5 (2003) 558–562.
[12] Z. Zhang, X.B. Ma, J. Zhang, F. He, S.P. Wang, J. Mol. Catal. A: Chem. 227 (2005) 141–146.
[13] D.N. Briggs, K.H. Lawrence, A.T. Bell, Appl. Catal. A 366 (2009) 71–83.
[14] I.J. Drake, K.L. Fujdala, A.T. Bell, T.D. Tilley, J. Catal. 230 (2005) 14–27.
[15] P.B. Zhang, Z. Zhang, S.P. Wang, X.B. Ma, Catal. Commun. 8 (2007) 21–26.
[16] D. C. Molzahn, M. E. Jones, G. E. Hartwell, J. Puga, US Patent 5,387,708, 1995.
[17] S.T. King, J. Catal. 161 (1996) 530–538.
[18] S.A. Anderson, T.W. Root, J. Catal. 217 (2003) 396–405.
[19] I.J. Drake, Y.H. Zhang, D. Briggs, B. Lim, T. Chau, A.T. Bell, J. Phys. Chem. B 110 (2006) 11654–11664.
[20] Y. Zhang, D.N. Briggs, E. de Smit, A.T. Bell, J. Catal. 251 (2007) 443–452.
[21] P. Serp, J.L. Figueiredo, Carbon Materials for Catalysis, John Wiley & Sons, Inc., Hoboken, 2009.
[22] M.L. Toebes, E.M.P. van Heeswijk, J.H. Bitter, A.J. van Dillen, K.P. de Jong, Carbon 42 (2004) 307–315.
[23] K.P. De Jong, J.W. Geus, Catal. Rev. 42 (2000) 481–510.
[24] P. Serp, M. Corrias, P. Kalck, Appl. Catal. A – Gen. 253 (2003) 337–358.
[25] P. Simonov, S. Troitskii, V. Likholobov, Kinet. Catal. 41 (2000) 255–269.
[26] M.L. Toebes, J.A. van Dillen, K.P. de Jong, J. Mol. Catal. A: Chem. 173 (2001) 75–98.
[27] H. Wang, R.T.K. Baker, US Patent 6,995,115, 2006.
[28] H. Wang, R.T.K. Baker, US Patent 7,001,586, 2006.
[29] J.S. Noh, J.A. Schwarz, J. Colloid Interface Sci. 130 (1989) 157–164.
[30] L.-W. Yin, M.-S. Li, D.-S. Sun, J.-J. Cui, Mater. Lett. 48 (2001) 21–25.
[31] M. Starsinic, R.L. Taylor, P.L. Walker Jr, P.C. Painter, Carbon 21 (1983) 69–74.
[32] P.E. Fanning, M.A. Vannice, Carbon 31 (1993) 721–730.
[33] T.G. Ros, A.J. van Dillen, J.W. Geus, D.C. Koningsberger, ChemPhysChem 3 (2002) 209–214.
[34] D. Alloyeau, B. Freitag, S. Dag, L.W. Wang, C. Kisielowski, Phys. Rev. B 80 (2009).
[35] C. Kisielowski, B. Freitag, M. Bischoff, H. van Lin, S. Lazar, G. Knippels, P. Tiemeijer, M. van der Stam, S. von Harrach, M. Stekelenburg, M. Haider, S. Uhlemann, H. Muller, P. Hartel, B. Kabius, D. Miller, I. Petrov, E.A. Olson, T. Donchev, E.A. Kenik, A.R. Lupini, J. Bentley, S.J. Pennycook, I.M. Anderson, A.M. Minor, A.K. Schmid, T. Duden, V. Radmilovic, Q.M. Ramasse, M. Watanabe, R. Erni, E.A. Stach, P. Denes, U. Dahmen, Microsc. Microanal. 14 (2008) 469–477.
[36] G.L. Curnutt, A. Dale Harley, Copper catalyzed oxidative carbonylation of methanol to dimethyl carbonate, in: A.E. Martell, D.T. Sawyer (Eds.), Oxygen Complexes and Oxygen Activation by Transition Metals, Plenum Press, New York, 1988, pp. 215–232.
[37] J.J. Byerley, E. Peters, Can. J. Chem. 47 (1969) 313–321.
[38] L.R. Radovic, J. Am. Chem. Soc. 131 (2009) 17166–17175.
[39] T.J. Bandosz, Surface chemistry of carbon materials, in: P. Serp, J.L. Figueiredo (Eds.), Carbon Materials for Catalysis, John Wiley & Sons, Inc., Hoboken, New Jersey, 2009, pp. 45–92.
[40] P.A. Simonov, A.V. Romanenko, I.P. Prosvirin, E.M. Moroz, A.I. Boronin, A.L. Chuvilin, V.A. Likholobov, Carbon 35 (1997) 73–82.
[41] J.L. Fulton, M.M. Hoffmann, J.G. Darab, Chem. Phys. Lett. 330 (2000) 300–308.
[42] J.L. Fulton, M.M. Hoffmann, J.G. Darab, B.J. Palmer, E.A. Stern, J. Phys. Chem. A 104 (2000) 11651–11663.

[43] I. Persson, M. Sandstrom, A.T. Steel, M.J. Zapatero, R. Akesson, Inorg. Chem. 30 (1991) 4075–4081.
[44] D.E. Etter, C.J. Wiedenheft, Sol. Energy Mater. 2 (1980) 423–431.
[45] T.G. Ros, D.E. Keller, A.J. van Dillen, J.W. Geus, D.C. Koningsberger, J. Catal. 211 (2002) 85–102.
[46] S. Hermans, C. Diverchy, O. Demoulin, V. Dubois, E.M. Gaigneaux, M. Devillers, J. Catal. 243 (2006) 239–251.
[47] D.M. Fenton, Pj. Steinwan, J. Org. Chem. 39 (1974) 701–704.
[48] P. Giannoccaro, N. Ravasio, M. Aresta, J. Organomet. Chem. 451 (1993) 243–248.
[49] A.F. Wells, J. Chem. Soc. (1947) 1670–1675.
[50] R.D. Willett, G.L. Breneman, Inorg. Chem. 22 (1983) 326–329.
[51] H. Finkbeiner, A.S. Hay, H.S. Blanchard, G.F. Endres, J. Org. Chem. 31 (1966) 549–555.
[52] B.T. Kilbourn, J.D. Dunitz, Inorg. Chim. Acta 1 (1967) 209–216.
[53] J.A. Bertrand, J.A. Kelley, Inorg. Chem. 8 (1969) 1982–1985.
[54] A.F. Wells, Z. Kristallogr. 100 (1938) 189–194.
[55] T. Hosokawa, M. Takano, S.I. Murahashi, J. Am. Chem. Soc. 118 (1996) 3990–3991.
[56] J.T. York, A. Llobet, C.J. Cramer, W.B. Tolman, J. Am. Chem. Soc. 129 (2007) 7990–7999.
[57] U. Romano, R. Tesei, M.M. Mauri, P. Rebora, Ind. Eng. Chem. Prod. Res. Dev. 19 (1980) 396–403.
[58] S.A. Anderson, S. Manthata, T.W. Root, Appl. Catal. A 280 (2005) 117–124.
[59] Y. Zhang, A.T. Bell, J. Catal. 255 (2008) 153–161.
[60] P. Koch, G. Cipriani, E. Perrotti, Gazz. Chim. Ital. 104 (1974) 599–605.
[61] M. Graziani, P. Uguaglia, G. Carturan, J. Organomet. Chem. 27 (1971) 275–278.
[62] F. Ragaini, Dalton Trans. (2009) 6251–6266.
[63] C. Amatore, S. Bensalem, S. Ghalem, A. Jutand, D. Fenech, A. Galia, G. Silvestri, C. R. Chim. 7 (2004) 737–746.
[64] H.F. Stoeckli, Carbon 28 (1990) 1.